FEATURE ARTICLE

Journal of Materials Chemistry
www.rsc.org/materials

# Solution-processed inorganic semiconductors

**David B. Mitzi**

*IBM T. J. Watson Research Center, P. O. Box 218, Yorktown Heights, NY 10598, USA. E-mail: dmitzi@us.ibm.com*

***Received 5th March 2004, Accepted 4th June 2004***
***First published as an Advance Article on the web 8th July 2004***



**The search for semiconductors that can be solution-processed into thin-film form at low temperature, while simultaneously providing quality device characteristics, represents a significant challenge for materials chemists. Continuous thin films with field-effect mobilities of 10 $cm^2 V^{-1} s^{-1}$ or greater are particularly desirable for high-speed microelectronic applications. Attainment of this goal should provide important opportunities for electronic devices, including potentially low-cost, large-area and flexible computing devices, displays, sensors and solar cells. While the majority of work toward this goal has focused on organic semiconductors (both molecular and polymeric), with highest reported mobilties in the range of 1 $cm^2 V^{-1} s^{-1}$, this review will address recent developments in the search for semiconductors with extended inorganic frameworks (offering the potential for higher mobility) that can be processed from solution using high-throughput, low-cost and low-temperature techniques such as spin-coating, printing or stamping. Two areas of recent interest will be highlighted – tin(II) iodide based organic–inorganic hybrids and soluble chalcogenide semiconductors. Application of the resulting thin films in devices will primarily be discussed in terms of thin-film field-effect transistors (TFTs), although other device applications can be envisioned.**

## Introduction

The ability to deposit and tailor high-quality semiconducting films and interfaces represents a critical component of modern microelectronics. Thin-film field-effect transistors (TFTs), for example, consist of thin p- or n-type semiconducting channel layers, with the conductivity modulated by application of a bias voltage to an adjacent but electrically isolated conducting gate. The electronic materials that comprise modern semiconducting devices are most commonly silicon-based, as a result of the relatively high mobility of the covalent silicon network and other desirable material properties (*e.g.*, the facile formation of an oxide with excellent insulating properties). However, they can also be considered from other families of materials that offer potential advantages over the silicon-based systems. The desire to deposit semiconducting films using low-cost (quick, low-temperature, non-vacuum) techniques, for example, has driven a search for alternative highly processible semiconductors. Deposition from solution is particularly attractive since it provides the possibility of employing a number of "soft" processes such as spin-coating, printing, and stamping, which in turn may enable new technologies (*e.g.*, flexible displays, electronic paper) or lower-cost conventional device fabrication.[1–14]

Among the numerous important characteristics of semiconductors that must be considered when exploring for new device materials, the carrier (electron/hole) mobility, $\mu$, is one key parameter, defined as the proportionality constant between the applied electric field and the corresponding average carrier drift velocity. The mobility is, in a more practical sense, related to the maximum switching speed achievable within a given electronic device configuration. Amorphous silicon, with a mobility of order 1 $cm^2 V^{-1} s^{-1}$, is sufficient for application in TFTs to address liquid crystal displays (LCDs).[15] Higher-speed logic applications require mobilities in the range of 10 $cm^2 V^{-1} s^{-1}$ or higher (*i.e.* as found in polycrystalline or single crystal silicon films).[16] The band gap is also an important semiconductor parameter since it directly relates to the intrinsic carrier density at room temperature. The bandgap, $E_g$, of most useful semiconductors ranges from a few tenths of an eV to 3 eV (for silicon, $E_g = 1.1$ eV). As channel materials for thin-film field-effect transistors (TFTs), semiconductors with too small a band gap will render the device difficult to shut off, while too large a band gap will make it impractical to inject sufficient charge in the channel to switch the device on (in the absence of doping). Note that injection of charge into the semiconductor depends on the relative positioning of the conduction and valence bands with respect to the Fermi energy of the metal contacts, as well as on the absolute value of the band gap.

Most recent attention on solution-processed semiconductors has focused on organic systems.[1–6] Mobilities as high as 0.89 $cm^2 V^{-1} s^{-1}$ have been achieved in p-type TFT channels comprised of solution-processed pentacene.[3] Analogous solution-processed n-type materials are less common than the p-type systems, with generally much lower mobilities.[5,6] While promising with regard to processing, cost, and weight considerations, molecular organic compounds typically have a number of disadvantages, including poor thermal and mechanical stability. In addition, while the electrical transport in organic materials has improved substantially over the last 15 years, the mobility appears to be fundamentally limited by the weak van der Waals interactions between organic molecules (as opposed to the stronger covalent and ionic forces found in

*David Mitzi is a research staff member in the Physical Sciences Department at the IBM T. J. Watson Research Center. He received a B.S.E. in Electrical Engineering (with a certificate in Engineering-Physics) from Princeton University in 1985 and a Ph.D. in Applied Physics from Stanford University in 1990. In 1990, he joined the Research Division at IBM and has since been examining the solid-state chemistry, as well as the thin-film deposition and device opportunities, for a variety of materials with interesting and potentially useful electronic properties.*

**David Mitzi**

DOI: 10.1039/b403482a

extended inorganic systems). Note that, in principle, soluble polymers might extend the mobility range of organic systems, because of the extended covalently-bonded framework. However, polymeric systems are difficult to purify and order into a crystalline film, significantly limiting the achievable mobilities.[2]

If thin-film mobilities greater than $>10\ cm^2\ V^{-1}\ s^{-1}$ could be achieved using a simple solution-processing technique, new technological opportunities might be envisioned, including low-cost logic for applications requiring higher levels of integration and speed than currently achievable with organic semiconductors. Ultimately, rather than a flexible display of moderate size (that might be enabled by current solution-processed materials with a mobility of order 1 $cm^2\ V^{-1}\ s^{-1}$), one might envision low-cost and flexible I/O screens or computers constructed entirely on plastic, with intelligence provided on the same surface as the display and with a potential for very large viewing area. Another important opportunity might be for low-cost "intelligent" sensor arrays (or similarly RFID tags) with locally-embedded logic (*e.g.*, to discriminate against false positives) and perhaps limited broadcasting capabilities.

The current review addresses efforts to solution-process inorganic semiconductors. The logic behind this approach is to take advantage of the covalently-bonded extended inorganic lattice to achieve higher mobility. Unfortunately, the typically poor solubility of the covalently-bonded inorganic framework represents a significant obstacle to attaining high quality films from solution. TFT channels based on the flow-directed assembly of solution-dispersed Si nanowires and CdS nanoribbons have recently been reported to yield high mobility.[7] These results, however, are for collections of discrete nanowires across the electrodes, rather than for a continuous film, and the quoted mobilities of $>100\ cm^2\ V^{-1}\ s^{-1}$ are based on an effective channel width calculated using the nanowire diameter multiplied by the number of wires crossing the channel. Use of the actual device channel width (the most useful comparison for thin-film devices) would, from the reported effective ($\sim 6\ S\ m^{-1}$) and uncorrected ($\sim 0.09\ S\ m^{-1}$) transconductances for the Si nanowire devices, yield a mobility approximately 2 orders of magnitude smaller than the reported values.

Alternative solution-based deposition processes, such as chemical bath,[8,9] galvanic deposition,[10] and successive ionic layer adsorption and reaction (SILAR)[11] have also been successfully used to form semiconducting chalcogenide-based films. The chemical bath technique, in particular, has yielded cadmium selenide films (after 40 min of multiple dipping and a final anneal at 400 °C) with mobility values as high as 15 $cm^2\ V^{-1}\ s^{-1}$.[8] Galvanic deposition is a related bath-based technique, wherein the driving force for deposition is established by the half-cell potential between a suitable anode and the cathode (typically the substrate).[10] SILAR involves alternately immersing a substrate into two (cation and anion) precursor solution baths, with intermediate water rinses to remove loosely bonded species, thereby building up the film in a layer-by-layer approach.[11] While these bath-based techniques are interesting examples of deposition from solution, they are generally not high-throughput processes, as a result of the relatively slow film growth in the chemical bath.

Here we will focus on two families of inorganic-based semiconductors that can be processed into thin, continuous, crystalline films using high-throughput processes, such as spin-coating or printing, and relatively low temperatures. Hybrid organic–inorganic perovskites[17] based on tin(II) iodide inorganic layers offer an unusual combination of good solubility in a wide range of common polar solvents and desirable semiconducting characteristics. TFTs with spin-coated hybrids as the semiconducting channel layer have yielded mobilities in the range of 1 $cm^2\ V^{-1}\ s^{-1}$, comparable to amorphous silicon, but with processing performed from solution and entirely at temperatures below 100 °C.[12,18,19] Soluble chalcogenides and chalcogenide precursors have also been used to prepare high quality semiconducting metal chalcogenide films. A recent report[13] describes a technique for spin-coating ultrathin semiconducting films with mobility values of order 10 $cm^2\ V^{-1}\ s^{-1}$, approximately an order of magnitude higher than previous spin-coated semiconductors and comparable to low-temperature polycrystalline silicon. In this review, we will address the solid state chemistry and the solution-based film deposition characteristics, as well as the promising TFT device results, enabled by these two materials classes.

## Organic–inorganic hybrids and related materials

Layered organic–inorganic perovskite structures are conceptually constructed from the three-dimensional (3D) $AMX_3$ perovskite by taking n-layer thick slices from along a selected crystallographic direction of the basic structure and stacking these slabs in alternation with organic cation layers (Fig. 1). Several possibilities for the inorganic slab orientation include <100>, <110>, and <111>.[20,21] Each of these structures consist of arrays of corner-sharing metal halide octahedra. Note that for both the <110>- and <111>-oriented families (Figs. 1b and 1c, respectively), continuous two-dimensional (2D) inorganic layers are only achieved for $n > 1$. The single

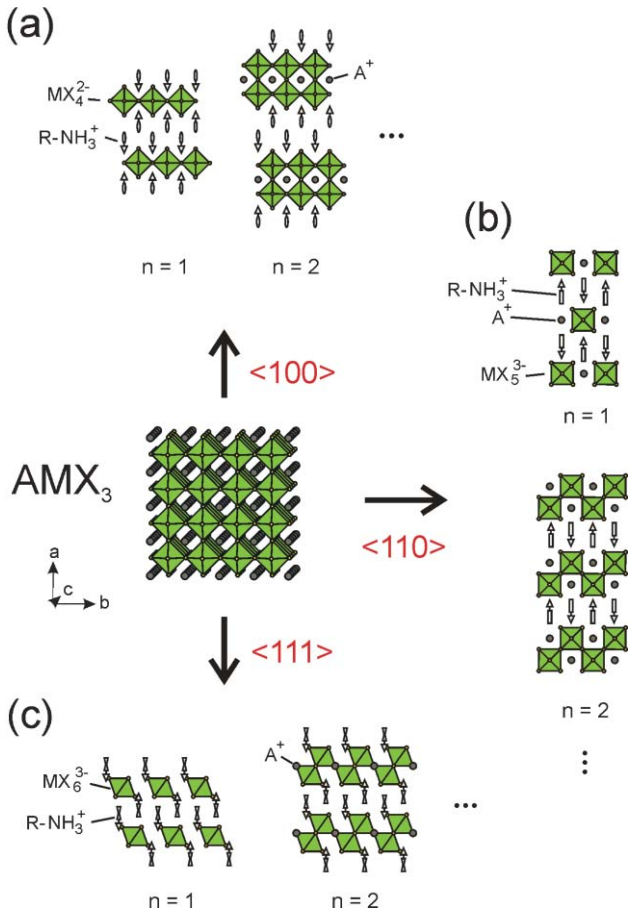


**Fig. 1** Three families of layered perovskites derived from the basic 3D $AMX_3$ structure by taking cuts from along different crystallographic directions: (a) $(R\text{–}NH_3)_2A_{n-1}M_nX_{3n+1}$ (<100>-oriented), (b) $(R\text{–}NH_3)_2A_nM_nX_{3n+2}$ (<110>-oriented), and (c) $(R\text{–}NH_3)_2A_{n-1}M_nX_{3n+3}$ (<111>-oriented). In each case, R is an organic moiety, A is a small organic cation (or monovalent inorganic cation), M is generally a divalent metal and X is a halide. The metal halide octahedral units, $MX_6$, are shown schematically in polyhedral representation. Adapted with permission from D. B. Mitzi, "Hybrid Organic-Inorganic Electronics," in *Functional Hybrid Materials* (Chapter 10), ed. P. Gómez-Romero and C. Sanchez. Copyright 2004 Wiley-VCH.

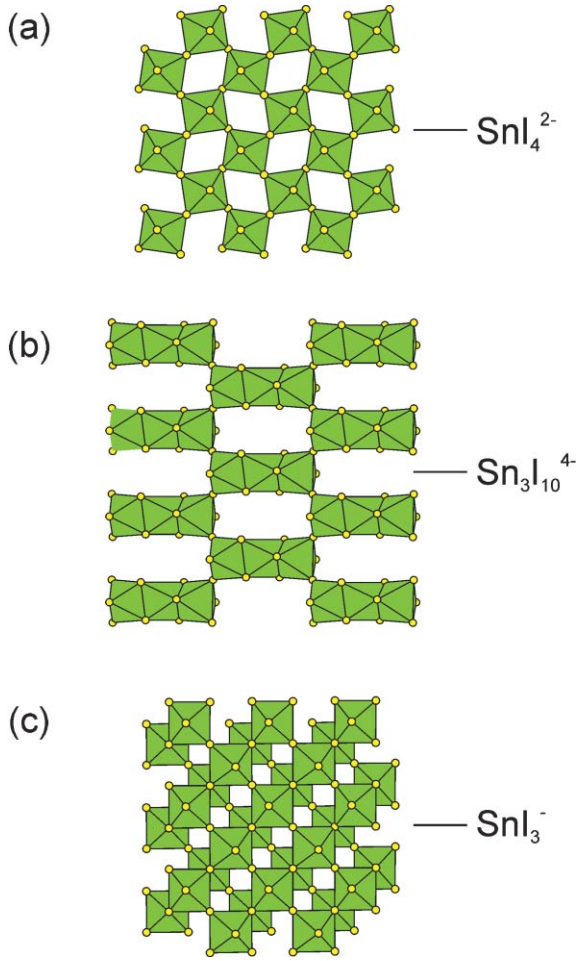


**Fig. 2** Representation of the inorganic framework connectivity for various layered tin(II) iodide based hybrids ($SnI_6$ moiety shown schematically in polyhedral representation): (a) single layer of corner-sharing $SnI_6$ octahedra ($n = 1$ <100>-oriented layered perovskite) in $[CH_3(CH_2)_{11}NH_3]_2SnI_4$, (b) single layer of corner-sharing and face-sharing distorted octahedra in $(Me_3PhN)_4(Sn_3I_{10})$,[29] and (c) double layer of corner-sharing and edge-sharing octahedra in $[CH_3(CH_2)_{11}NH_3]SnI_3$.[30]

layer ($n = 1$) <100>-oriented layered perovskites are the simplest and most widely considered perovskites and contain single $MX_4^{2-}$ layers, where M is a divalent metal (*e.g.*, $Cu^{2+}$, $Ni^{2+}$, $Co^{2+}$, $Fe^{2+}$, $Mn^{2+}$, $Cr^{2+}$, $Pd^{2+}$, $Cd^{2+}$, $Ge^{2+}$, $Sn^{2+}$, $Pb^{2+}$, $Eu^{2+}$, or $Yb^{2+}$) and X is a halide (*e.g.*, $Cl^-$, $Br^-$, $I^-$). The single-layer perovskite family has been recently extended to include higher-valent metal halide sheets (*e.g.*, $Bi_{2/3}I_4^{2-}$, $Sb_{2/3}I_4^{2-}$), with appropriately chosen organic cation layers templating the metal-deficient inorganic layers.[22] This review will focus on the tin(II) halide based hybrid perovskites (particularly iodide-based systems) and related structures due to their unusual semiconducting properties and high degree of solubility.[20,23–28]

Each of the layered perovskite structures described above contain layers of *corner-sharing* metal halide octahedra (Fig. 2a). Several other interesting layered tin(II) iodide based systems have recently been reported. In the compound, $(Me_3PhN)_4(Sn_3I_{10})$, for example, combinations of *corner-* and *face-shared* highly-distorted octahedra yield $Sn_3I_{10}^{4-}$ layers (Fig. 2b).[29] $[CH_3(CH_2)_{11}NH_3]SnI_3$ consists of a lamellar structure with well-connected $SnI_3^-$ double layers of both *corner-* and *edge-sharing* tin(II) iodide octahedra (Fig. 2c), isotypic to that of $MoO_3$.[30] The key aspect of each of these structures is the existence of 2D semiconducting sheets. Note that zero-dimensional (0D) structures (*i.e.* those with isolated tin iodide species), when deposited as thin films, do not provide

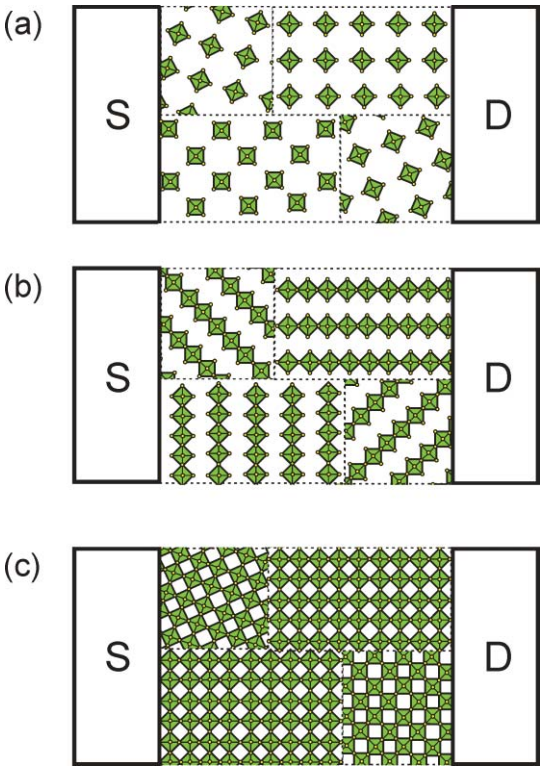


**Fig. 3** Connectivity of the inorganic framework between electrical contacts for thin-film polycrystalline hybrids based on (a) zero-dimensional (0D), (b) one-dimensional (1D), and (c) two-dimensional (2D) inorganic frameworks. The tin(II) iodide framework is shown schematically using green octahedra (representing $SnI_6$). The organic component of the structure is not drawn for clarity. Dashed lines indicated grain boundaries.

a continuous path between prospective device contacts through the inorganic framework (Fig. 3a). Similarly, one-dimensional (1D) structures require alignment of the inorganic chains (often difficult) so that they can extend between contacts (Fig. 3b). While 3D frameworks span the contacts, the more rigid structure limits the size, type and functionality of organic cations that can fit within the structure. Two-dimensional systems are therefore a convenient choice for devices based on thin organic–inorganic semiconducting films (Fig. 2c). The large repertoire of layered inorganic frameworks (both perovskite and other related structures) and potential for substitutions on either the metal or halogen site enable substantial tailoring of the electronic and optical properties of the tin(II) iodide framework.[17]

The organic cation layers provide even more extensive flexibility for the hybrid perovskite structures. For the <100>-oriented layered perovskites, the organic cations generally contain either one ($R–NH_3^+$) or two ($^+H_3N–R–NH_3^+$) ammonium groups (Fig. 4), which tether to the halides in the adjacent inorganic sheets, and an organic tail (R) that extends within the space between layers. For monoammonium cations, the ammonium group interacts with a single inorganic layer through hydrogen and ionic bonding. The organic tail extends into the space between the layers and a van der Waals gap separates the bilayer of organic tails from adjacent layers (in some cases, however, there is interdigitation of the organic tails from adjacent layers). While in most cases this van der Waals gallery is empty, recently structures have been reported with benzene or hexafluorobenzene intercalated within the van der Waals gap, held in place by a fluoroaryl–aryl interaction (Fig. 4c).[31] For diammonium cations, each organic cation spans the entire distance between layers, interacting with two adjacent inorganic layers through the ammonium groups attached at each end.

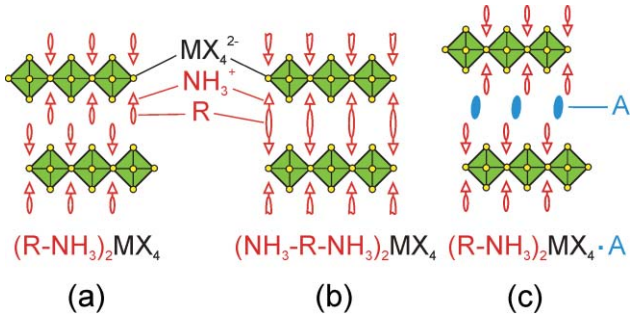


**Fig. 4** Schematic representation of single-layer <100>-oriented perovskites with (a) monoammonium ($R–NH_3^+$) or (b) diammonium ($^+H_3N–R–NH_3^+$) organic cations. In (c) organic molecules are intercalated in the van der Waals gap of the monoammonium-based systems [*e.g.*, $(C_6H_5C_2H_4NH_3)_2SnI_4{\cdot}(C_6F_6)$ or $(C_6F_5C_2H_4NH_3)_2SnI_4{\cdot}(C_6H_6)$]. Adapted from *J. Chem. Soc., Dalton Trans.*, 2001, 1 (ref. 21) by permission of the Royal Society of Chemistry.

In addition to alkylammonium and simple arylammonium cations, the structural constraints of the perovskite family provide sufficient flexibility to incorporate more complex and functional organic cations, such as oligothiophene-based amines[32,33] and 1-pyrenemethylamine,[34] which have a smaller HOMO–LUMO separation than the less complex molecules. Recently, examples of mixed organic cations have also been demonstrated, enabling the combining of functionality in the organic layer of the structure.[35] Note that the organic cations serve to both template or tailor the formation of the inorganic layers (thereby controlling the electronic properties of the layers),[21,36] as well as to potentially facilitate film formation during solution processing. While typically protonated primary amine groups act to template the formation of the inorganic layers, 2,2′-biimidazolium and the quaternary-ammonium-containing cation 2-trimethylammonioethylammonium ($[Me_3NCH_2CH_2NH_3]^{2+}$) have also recently been reported to function as the templating agent in the tin(II) iodide based perovskites.[37,38]

Unlike most halide salts, which yield insulating electrical character, the halide-based perovskite families, $(R–NH_3)_2(CH_3NH_3)_{n-1}Sn_nI_{3n+1}$ and $[NH_2C(I)=NH_2]_2(CH_3NH_3)_nSn_nI_{3n+2}$, exhibit a semiconductor–metal transition as a function of increasing perovskite layer thickness (Fig. 5), as well as a potential for high carrier mobilities.[20,23] The

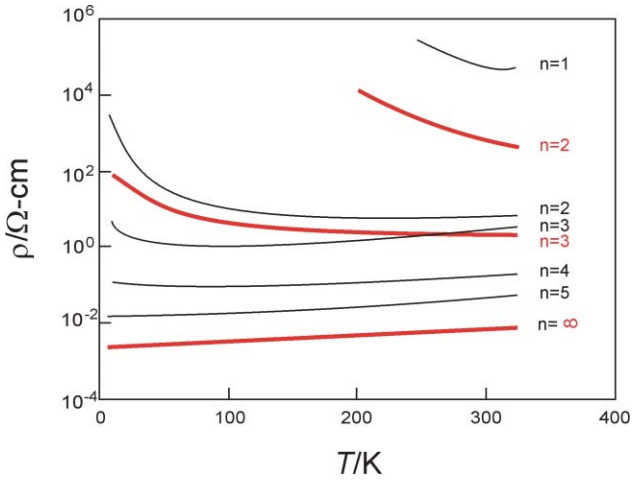


**Fig. 5** Resistivity ($\rho$) as a function of temperature for pressed pellet samples of the layered perovskite families $(C_4H_9NH_3)_2(CH_3NH_3)_{n-1}Sn_nI_{3n+1}$ (black curves) and $[NH_2C(I)=NH_2]_2(CH_3NH_3)_nSn_nI_{3n+2}$ (red curves), as well as for the $n \rightarrow \infty$ end-member of both families ($CH_3NH_3SnI_3$). Adapted with permission from *Science*, 1995, **267**, 1473 (ref. 20). Copyright 1995 American Association for the Advancement of Science.

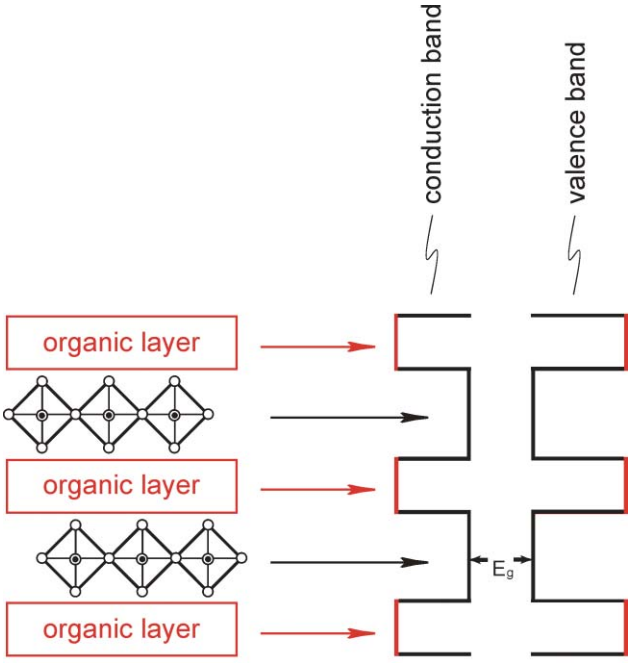


**Fig. 6** Schematic organic–inorganic perovskite structure and the most common resulting energy level arrangement. Semiconducting tin(II) iodide sheets alternate with organic layers having much wider bandgap (HOMO–LUMO separation), resulting in a type I quantum well structure. By appropriate choice of inorganic framework and organic layers other energy level schemes can be envisioned. Adapted with permission from *IBM J. Res. Dev.*, 2001, **45**, 29 (ref. 18).

three-dimensional perovskite, $CH_3NH_3SnI_3$, for example (the $n \rightarrow \infty$ member of both above-mentioned families), is a low carrier density p-type metal with a Hall hole density of $1/R_he \approx 2 \times 10^{19}$ cm$^{-3}$ and a Hall mobility of $\mu \approx 50$ cm$^2$ V$^{-1}$ s$^{-1}$ at room temperature.[27] The high degree of conductivity derives from the large dispersion of the Sn(5s) band [hybridized with I(5p)] along the <111> direction of the cubic Brillouin zone, leading to a marginal crossing of the Sn(5s) and Sn(5p) bands near the R point ($2\pi[½, ½, ½]/a$), with the Fermi energy falling roughly between the two bands. With reduced dimensionality of the tin iodide framework (*e.g.*, for smaller $n$), the band gap widens, yielding a semiconducting material. The $n = 1$ structure, for example, has a band gap of order 2.2 eV (quite appropriate for TFT applications).[28] The organic cation can be used to fine-tune the value of the band gap indirectly through its impact on the inorganic structure (*e.g.*, hydrogen bonding and steric interactions of the organic cation influence the Sn–I–Sn bond angle).[35,36,38,39] The layered hybrid perovskites can also be viewed as multilayer quantum well structures (Fig. 6), with semiconducting inorganic sheets alternating with wider band gap (*i.e.* HOMO–LUMO gap) organic layers.[18] Making substitutions on either the metal or halogen site modifies the band gap of the inorganic layers (well depth), while the width of the barrier and well layers can easily be adjusted by changing the length of the organic cations and the number of perovskite sheets between each organic layer, respectively. The self-assembling quantum well structures are expected to share many of the interesting electronic characteristics of structures prepared by "artificial" techniques, such as molecular beam epitaxy (MBE), with however the advantage of atomically smooth interfaces (*i.e.*, single crystals of the quantum well structures can readily be prepared from solution).[40]

In addition to desirable electrical transport characteristics, the tin(II) iodide based perovskites exhibit remarkable solubility in a range of common polar solvents (*e.g.*, hydriodic acid, alcohols, acetone, acetonitrile, *N*,*N*-dimethylformamide), enabling a variety of high-throughput solution-based film deposition techniques, including spin-coating, stamping and

printing. Organic–inorganic perovskite films have recently been formed, for example, using the Langmuir–Blodgett (LB) technique, which in principle provides the possibility of thickness control at the monolayer level.[41]

Spin-coating is a very rapid solution-based process for depositing thin films on a variety of substrates, including glass, quartz, sapphire, silicon and plastic. The process involves preparing a solution of the hybrid with the desired concentration, applying a quantity of the solution to a substrate and then spinning the substrate. As the solution spreads, it dries and leaves a film of the hybrid. Parameters for the deposition include the choice of substrate, deposition temperature, the solvent (*e.g.*, viscosity, vapor pressure, wetting characteristics), the concentration of the hybrid in the solvent, and the spin speed. Post-deposition, low-temperature annealing ($T < 100$ °C) of the films is also sometimes employed to remove excess solvent and to improve crystallinity and phase purity. Spin-processed $n = 1$ layered perovskite films based on a tin(II) iodide framework are generally very smooth (mean roughness ~1–2 nm), crystalline, and highly oriented, as is desirable for use in device structures. The inherent air-sensitivity of the tin(II) iodide based systems implies that all spin processing must be performed under rigorously inert atmosphere conditions.

As an example, films of several phenethylammonium-based tin(II) iodide compounds have been fabricated by spin-coating.[36] The series consists of hybrids prepared using a phenethylammonium cation and analogous cations with a fluorine substituted at the 2- or 3-position on the phenyl ring. Spinning was performed by flooding the quartz substrate with solution (20 mg of the recrystallized perovskite in 1.6 mL of freshly dried/distilled methanol) and ramping to 3000 rpm. The resulting films exhibit well-defined X-ray diffraction peaks corresponding to the (*h*00) series of reflections (Fig. 7), indicating good crystallinity and a high degree of preferred orientation. Analogous films deposited on silicon using the same conditions as described above are approximately 20(3) nm thick, as measured using an AFM scan across a scratch in the film. Note that this corresponds to ⩽10 unit cells thick, demonstrating the very thin nature of these films.

Grain structure is crucial for device properties and can be controlled by the choice of organic cation in the hybrid structure. In the above films, for example, the position of fluorine substitution on the phenyl ring has a pronounced effect on the grain structure.[36] Fluorine substitution on the 3- and 4-positions of the phenethylammonium (PEA) cation yields films with a larger grain structure (~150–200 nm) (Fig. 8a)

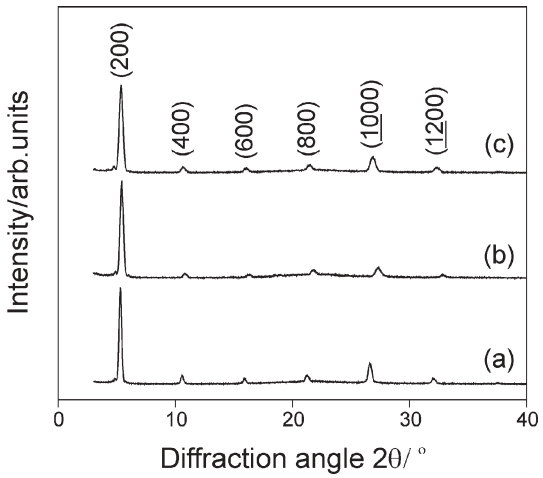


**Fig. 7** Powder X-ray patterns for spin-coated thin films of the $(R–NH_3)_2SnI_4$ hybrid perovskites (Cu Kα radiation), where $R–NH_3$ = (a) 3-fluorophenethylammonium, (b) phenethylammonium, and (c) 2-fluorophenethylammonium. The X-ray reflection indices given above the data for sample (c) are the same for each sample.

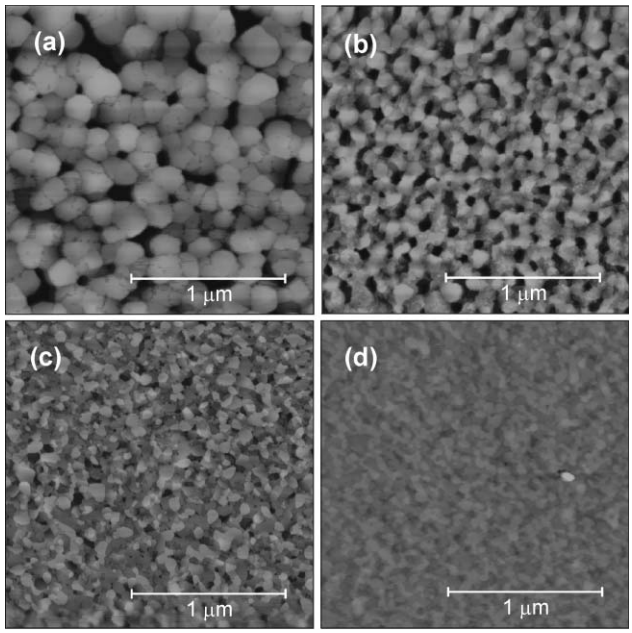


**Fig. 8** Atomic Force Microscopy (AFM) topology images for spin-cast films of $(R–NH_3)_2SnI_4$ hybrid perovskites, where $R–NH_3$ = (a) 3-fluorophenethylammonium, (b) phenethylammonium, (c) 2-fluorophenethylammonium, and (d) 2-chlorophenethylammonium.[36,39] Each film is on a silicon substrate with 5000 Å of thermally grown oxide. Adapted from *Chem. Mater.*, 2001, **13**, 3728 (ref. 36). Copyright 2001 American Chemical Society.

relative to that for the unsubstituted phenethylammonium tin(II) iodide films (Fig. 8b), given similar spin conditions. In contrast, fluorine substitution at the 2-position leads to a significantly smaller grain structure (<100 nm) (Fig. 8c) than that for the unsubstituted system. The changes in film morphology in the current samples might either arise from the different solubility of the organic cations as a function of the position of the fluorine substitution (2-FPEA is more soluble than 4-FPEA in many polar solvents) or from variations in the cation-substrate interactions (in this case, the fluorine atom should interact with the substrate surface in the 3-FPEA and 4-FPEA systems, but not in the PEA or 2-FPEA systems). Note that a film with chlorine replacing fluorine at the 2-position of the phenethylammonium cation (2-ClPEA) yields very similar grain morphology to the fluorine analog (Fig. 8d).[39] Changing the solvent can also have a dramatic affect on the grain structure and size. Methanol solutions were chosen in the present examples because the resulting continuous films consisted of reasonable-sized and well-connected crystallites.

For electronic circuit fabrication, the ability to pattern thin films is crucial to define the active area of the device. Recently, a low-temperature and parallel process has been demonstrated using microcontact printed templates to pattern subsequently spin-coated hybrid materials.[42] The technique consists of preparing a polydimethylsiloxane (PDMS) stamp with desired topographies and "inking" the stamp with a molecular species comprised of a head group that binds to the substrate surface and a hydrophobic tail group that directs the deposition of the solution-deposited hybrid material. Alkyl- and fluorinated alkyltrichlorosilane "inks" are suitable for $SiO_2$. Alkylphosphonic acids are used on $SiO_2$ or $ZrO_2$ and hydroxamic acids are used on $ZrO_2$ to provide the appropriate head groups for the given substrate. The inked PDMS stamp is briefly (30–60 s) brought into conformal contact with the substrate surface and removed, transferring the chemical ink to the oxide surface in a pattern defined by the stamp topography. The hybrid semiconductor can then be deposited on the patterned surface using a spin-coating (or other solution-based) process as described above. During spinning, regions of the substrate that are

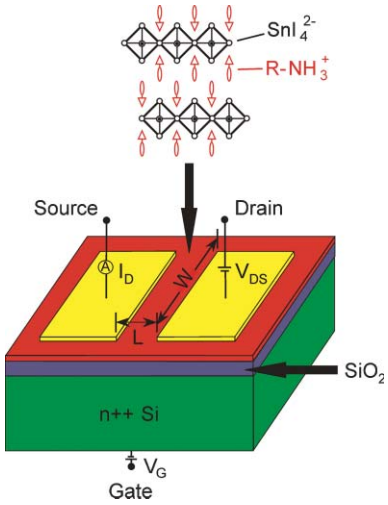


**Fig. 9** Schematic diagram of a TFT device structure employing a layered organic–inorganic perovskite as the semiconducting channel.

covered with the hydrophobic molecular ink de-wet while the hydrophilic bare oxide surface is effectively covered by the evaporating solution. In this way, effective patterning during solution processing can be achieved, with a resolution of at least 3 μm.[42] The additive nature of this process (as opposed to traditional lithography, which generally requires patterning and removal of material) has the attractive feature that the organic–inorganic semiconducting materials are not exposed to potentially harmful post-deposition processing.

The relatively high electrical mobility, combined with the ability to conveniently solution process and pattern the hybrids, renders the tin(II) iodide based perovskites an interesting family to consider for use in TFT channels. Fig. 9 depicts a typical bottom-gate organic–inorganic TFT configuration.[12,18,19] The device operates by modulating the surface charge density in the semiconducting channel (between the source and drain), by application of a bias voltage to the gate. Thin films of the hybrid perovskite are spin-coated from a methanol solution, in an inert atmosphere, onto thermally oxidized, degenerately n-doped silicon wafers (which also act as the gate electrode). The $SiO_2$ layer acts as the gate insulator. High work function metals, such as Pd, Au, or Pt, are deposited by e-beam evaporation through silicon membrane masks and serve both as the source and drain electrodes and to define the channel dimensions. The organic–inorganic perovskite is spin-coated after depositing the source and drain electrodes to prevent exposing the hybrid perovskite films to potentially harmful metal deposition conditions (*e.g.* high temperatures or oxygen/moisture). The perovskite semiconductor films are simply patterned using a solvent-soaked cotton swab to remove material from around each device. By isolating the devices, leakage current between source/drain electrodes and the back gate is effectively avoided. Patterning can also be accomplished using a microcontact printed template to pattern spin-coated hybrid materials.[42]

Fig. 10 shows representative device characteristics for a TFT with the organic–inorganic perovskite $(C_6H_5C_2H_4NH_3)_2SnI_4$ [$(PEA)_2SnI_4$] as the channel layer. The tin(II) iodide based perovskite film forms a p-channel transistor, consistent with previous Hall measurements.[23,27] Application of a negative bias to the gate electrode ($V_G < 0$) increases the number of majority holes in the semiconducting channel contributing to the drain current ($I_D$). These devices show typical transistor-like behavior, as $I_D$ increases linearly at low source-drain voltage ($V_D$) and then saturates as $V_D$ increases and the holes in the channel are pinched-off near the drain electrode (Fig. 10a). Fig. 10b shows the dependence of $I_D$ *versus* $V_G$, at $V_D = -100$ V. As determined from these curves using

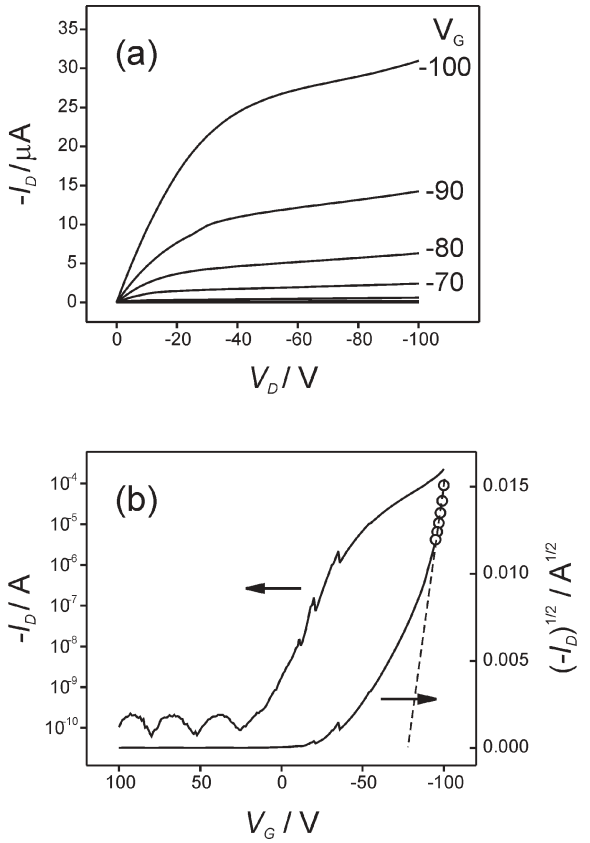


**Fig. 10** (a) Drain current, $I_D$, *versus* drain voltage, $V_D$, as a function of gate voltage, $V_G$, for a TFT with a spin-coated channel of $(C_6H_5C_2H_4NH_3)_2SnI_4$, a channel length $L = 15$ μm, and a channel width $W = 1500$ μm. The gate dielectric is 5000 Å of $SiO_2$. (b) Plots of $I_D$ and $I_D^{1/2}$ *versus* $V_G$ at constant $V_D = -100$ V.

standard device-modeling equations,[6] the saturation regime field-effect mobility for the device is $\mu_{sat} = 1.1$ cm$^2$ V$^{-1}$ s$^{-1}$ and the $I_{ON}/I_{OFF}$ ratio is $\sim 10^6$. The device characteristics exhibit substantial variability from device to device, primarily as a result of the reactivity of the tin(II) iodide based films and the strong dependence on film quality. Saturation-regime mobility typically ranges from 0.2–1.4 cm$^2$ V$^{-1}$ s$^{-1}$ for the spin-coated devices based on phenethylammonium tin(II) iodide, comparable to the performance of amorphous silicon and state-of-the-art vacuum-deposited organic semiconductors. Similar device characteristics (*i.e.* $\mu$ and $I_{ON}/I_{OFF}$) are achieved at substantially lower applied voltages for devices fabricated using a thinner or high dielectric constant gate insulator.[19]

The mobility discussed above represents the mobility in the saturation regime. In fact, the mobility is gate voltage dependent[12,18,19] as a result of trap states in the band gap (also observed in organic and amorphous silicon).[6,43] At low gate bias, there are more trap states than carriers and transport is *via* hopping between localized trap states, yielding a lower mobility. As the gate bias is made progressively more negative (for a p-channel device), the trap states are filled until ultimately (when they are all filled) additional carriers can transport with the intrinsic mobility of the semiconductor. For the spin-coated tin(II) iodide based hybrids, the mobility in the linear regime is also typically an order of magnitude smaller than that in the saturation regime. For the $(PEA)_2SnI_4$-based device employed in Fig. 10, the linear regime mobility is $\mu_{lin} = 0.07$ cm$^2$ V$^{-1}$ s$^{-1}$. Much higher linear regime mobilities have been achieved in melt-processed hybrid films,[44] highlighting the importance of controlling grain structure (the melt-processed films generally have larger and better-connected grains).

The initial results described above for the spin-coated hybrid semiconductors provide mobilities that are in the range of the

best vacuum-deposited organic semiconductors and amorphous silicon and are, perhaps more significantly, among the best reported results for semiconductors that can be spin-coated from solution at ambient temperatures. Given the higher mobilities observed for perovskite films deposited using low-temperature melt-processing (as high as 2.6 $cm^2\ V^{-1}\ s^{-1}$ in the saturation regime and 1.7 $cm^2\ V^{-1}\ s^{-1}$ in the linear regime),[44] better performance is presumably also possible for the solution-processed devices as more is learned about controlling the grain structure of the deposited films. In addition, while the tin(II) iodide systems are examples of p-type semiconductors, the identification of soluble n-type analogs is desirable to enable complementary logic. A further issue to address involves the air/moisture sensitivity of the current generation of tin(II) iodide based semiconductors, which necessitates that all processing and device operation be performed under rigorously inert atmosphere conditions. Materials issues, such as those described above, can likely be overcome as new inorganic frameworks and processing techniques are explored within the perovskite family and among other organic–inorganic hybrid semiconductors. Recently, for example, solution-deposited thin films of tetrakis((*S*)-1-amino-3,7-dimethyloctane)platinum(II) tetrachloroplatinate(II), $[Pt(NH_2dmoc)_4][PtCl_4]$, a hybrid compound with a structure consisting of quasi-one-dimensional semiconducting chains of linearly-arranged platinum atoms, have been demonstrated.[45] The highly-oriented films, deposited on friction-deposited transfer films of poly(tetrafluoroethylene) (PTFE), yielded field-effect mobilities as high as $10^{-3}$–$10^{-4}$ $cm^2\ V^{-1}\ s^{-1}$ (p-type). While these values are not as high as for the hybrid perovskites, the platinum compounds yield exceptional environmental stability and can even be subjected to hot water treatment without device degradation.

## Soluble chalcogenides

While the metal halide based hybrid semiconductors are attractive because of their good solubility and useful semiconducting properties, metal chalcogenides are also interesting systems for device fabrication, currently being actively considered for use in TFTs,[7–9,13,14] solar cells,[46,47] thermoelectric[48,49] and phase change memory[50–53] applications. The covalent nature of the metal chalcogenide framework leads to the possibility of high mobility, with additional opportunities for identifying both n-type and p-type semiconductors and convenient band gaps for device fabrication (Table 1).[54–59] Unfortunately, while the potential for higher mobility exists, the increased covalency of the extended metal chalcogenide systems also reduces their solubility, rendering simple and low-cost film deposition a significant challenge. Thermal evaporation, sputtering and chemical vapor deposition (CVD) are among the most common techniques employed for deposition of chalcogenide films. These techniques require either high vacuum conditions, which are not amenable to high-throughput or large-area applications, or high temperatures, which are not conducive to low-temperature flexible plastic substrates.

Spray pyrolysis is one currently employed high-throughput technique that involves spraying a solution, which contains a soluble salt of the metal (*e.g.*, metal chloride), along with a source of the chalcogen (*e.g.*, thiourea, thioacetamide, selenourea), onto a heated substrate (generally in the range 250–450 °C).[60–62] In some cases, a complexing agent (*e.g.*, acetic acid, tartaric acid) is also added to the solution to prevent precipitation of the metal chalcogenide before spraying.[62] While metal chalcogenide films are formed using this technique, with examples including $ZnS_xSe_{1-x}$, $CuInS_2$, $Sb_2S_3$, $Sb_2Se_3$, the films often have substantial impurities of halogen, carbon or nitrogen. Annealing in reducing atmospheres of $H_2$ or $H_2S$ at temperatures up to 450 °C can be used to reduce the level of impurities in the film, but these relatively aggressive treatments are not compatible with a wide range of substrate materials, and/or require specialized equipment.

**Table 1** Mobility and band gap data for selected metal chalcogenide semiconductors[b]

| Semiconductor | Electron mobility/ $cm^2\ V^{-1}\ s^{-1}$ | Hole mobility/ $cm^2\ V^{-1}\ s^{-1}$ | Band Gap/eV[a] | Ref. |
|---|---|---|---|---|
| $SnS_2$ | 18 | | 2.1 i | 54,55 |
| $SnSe_2$ | 27 | | 1.0 i | 54 |
| CdS | 250 | | 2.4 d | 56 |
| CdSe | 650 | | 1.7 d | 56 |
| ZnSe | 600 | | 2.7 d | 56 |
| ZnTe | | 100 | 2.2 d | 56 |
| InS | 50 | | 1.9 i | 59 |
| $CuGaS_2$ | | 15 | 2.5 d | 58 |
| $CuInS_2$ | 200 | 15 | 1.5 d | 58 |
| $CuGaSe_2$ | | 20 | 1.7 d | 58 |
| $AgInS_2$ | 150 | | 2.0 d | 58 |
| $CdGa_2Se_4$ | 33 | | 2.2 i | 57 |
| $HgGa_2Se_4$ | 400 | | 1.8 i | 57 |
| $ZnIn_2Se_4$ | 35 | | 1.7 i | 57 |
| $CdIn_2Se_4$ | 22 | | 1.6 i | 57 |

[a] i = indirect; d = direct gap. [b] Note that mobility values (and in some cases even carrier type) are strongly dependent on small changes in sample stoichiometry. As the metal chalcogenides often accommodate substantial variation in stoichiometry, the listed values should be considered as representative.

Recently, $MX_2$ (M = Nb, Ta, Mo, W, Sn, Ti; X = S, Se) films have been solution processed using a technique based on forming ultrathin platelets through Li intercalation and exfoliation in water, followed by self-assembly of the platelets at a water/organic solvent interface and transfer of the platelets to a dipped hydrophilic substrate (Fig. 11).[63,64] The resulting films are ultrathin (5–10 nm), generally with a high work function (4.4–5.9 eV), and have been used as electrodes for organic light-emitting devices (OLEDs).[64] The high work function of the metal chalcogenides reduces the hole injection barrier into the organic light-emitting device layer, enabling promising electrical characteristics.

Several efforts to spin-coat chalcogenide films have recently been reported. CdSe semiconducting films were cast, for example, using a soluble precursor of organic derivatized CdSe nanocrystals.[14] This technique, however, requires the formation of nanocrystals with tight control on particle size distribution in order to enable effective sintering during a postdeposition thermal treatment. The particle control requires repeated dissolution and centrifugation steps in order to isolate a suitably uniform collection of nanocrystals. TFTs, based on solution cast films that were annealed at 350 °C for 1 h, yielded transistor-like device characteristics with a mobility of $\sim 1\ cm^2\ V^{-1}\ s^{-1}$. The devices prepared using this technique, however, exhibited unusual features, including substantial device hysteresis and a negative resistance in the saturation regime, perhaps as a result of trap or interface states either within the semiconducting film or at the interface between the semiconductor and the insulator.

Dhingra *et al.*[65] have demonstrated a soluble precursor for metal chalcogenides that can be used to spin-coat films of the corresponding metal chalcogenide (*e.g.*, CdSe, $Cu_{2-x}Se$, β-$In_2Se_3$, TlSe and $CuInSe_2$). However, in this process, the quaternary ammonium or phosphonium polyselenide species used to solublize the chalcogenide framework, which ultimately decompose from the sample during a heat treatment, are bulky and much of the film disappears during the annealing sequence (*i.e.* 70–87%). The large percentage of the sample that is lost during the thermal treatment suggests that the technique is most appropriate for thick films, since thin films would likely be rendered discontinuous during the decomposition step (the

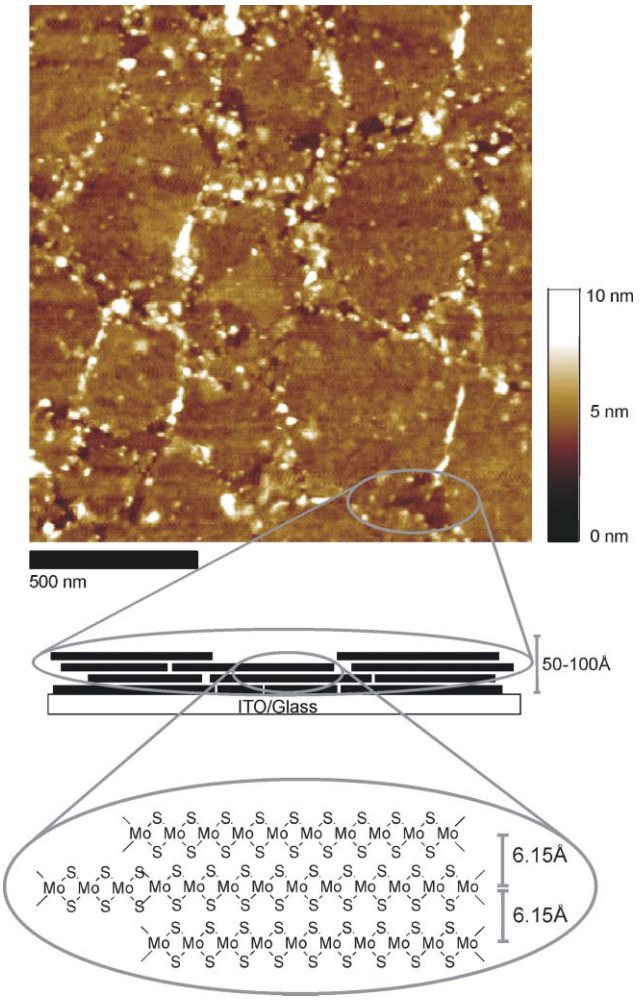


**Fig. 11** AFM micrograph and schematic diagram of a $MoS_2$ film deposited on a glass substrate. The AFM image reveals a number of $MoS_2$ platelets, aligned with the *c*-axis perpendicular to the substrate, with good coverage across the substrate surface. The schematic represents the platelet ordering on the substrate, with individual platelets stacking randomly in the *ab*-plane, but always with constant 6.15 Å steps along the *c*-axis. Reproduced with permission from G. L. Frey, K. J. Reynolds and R. H. Friend, *Adv. Mater.*, 2002, **14**, 265 (ref. 64). Copyright 2002 Wiley-VCH.

above mentioned study considered films with thickness ~25–35 μm). Additionally, relatively high temperatures are required for the thermal decomposition of the polyselenides (~530 °C), making this process incompatible with even the most thermally robust plastic substrates (*e.g.*, Kapton sheet can withstand temperatures as high as 400 °C). Films of crystalline $MoS_2$ have also been spin-coated from a solution of $(NH_4)_2MoS_4$ in an organic diamine.[66] However, high-temperature post-deposition anneals are again required to achieve crystalline films (600–800 °C).

Recently, we reported the use of hydrazine as a solvent for main group metal chalcogenides (*e.g.*, $SnS_{2-x}Se_x$) and the subsequent processing and characterization of crystalline thin films based on these solutions.[13] The simple approach employs excess chalcogen (S or Se) to directly improve the solubility and film-forming properties of selected main group metal chalcogenides in hydrazine, as a result of the formation of highly soluble hydrazinium-based precursors. For the tin(IV) chalcogenides, dissolution is expected to primarily occur through the overall reaction:

$$5N_2H_4 + 2X + 2SnX_2 \rightarrow N_2\,(gas) + 4N_2H_5^+ + Sn_2X_6^{4-}\ (X = S, Se) \quad (1)$$

The pale yellow coloration of the solution suggests at most a

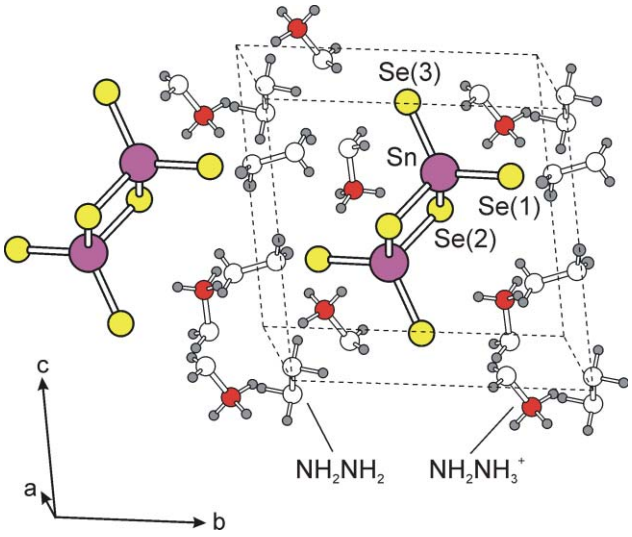


**Fig. 12** $(N_2H_4)_3(N_2H_5)_4Sn_2Se_6$ crystal structure determined using single crystal X-ray diffraction.[68] Unit cell (outlined by dashed lines): Triclinic ($P\bar{1}$), $a$ = 6.6475(6) Å, $b$ = 9.5474(9) Å, $c$ = 9.883(1) Å, $\alpha$ = 94.110(2)°, $\beta$ = 99.429(2)°, $\gamma$ = 104.141(2)°, $V$ = 595.9(1) Å$^3$, and $Z$ = 1. Nitrogen atoms with two attached hydrogens are drawn as unfilled circles, while those with three attached hydrogens are drawn as red-shaded circles.

low concentration of polychalcogenide anions[67] and vigorous bubbling during dissolution supports the gas generation indicated in Eqn. (1). Evaporation of the solution over a 24 hour period yields $(N_2H_5)_4Sn_2S_6$ (X = S) or $(N_2H_4)_3(N_2H_5)_4Sn_2Se_6$ (X = Se) crystals, which consist of anionic dimers of edge-sharing $SnX_4$ tetrahedra ($Sn_2X_6^{4-}$) alternating with hydrazinium cations and, for X = Se, neutral hydrazine molecules (Fig. 12).[13,68] The observed crystal structures are similar to that found[69] in $K_4Sn_2Se_6$ with, however, the replacement of the alkali metal cation with a small volatile hydrazinium species, which can be decomposed from the material using a low temperature anneal. Upon heating, the decomposition to the microcrystalline metal chalcogenide semiconductor is essentially complete by approximately 200 °C, highlighting the low-temperature nature of this process.[13]

Continuous crystalline semiconducting tin chalcogenide films as thin as 50 Å can be formed by spin-coating the hydrazine-based solutions of $SnS_2$ and $SnSe_2$ (with added sulfur).[13] The solutions are spun onto cleaned hydrophilic substrates. The resulting hydrazinium precursor films are decomposed at low-temperature (<300 °C) using a short (~20 min) anneal. The low-temperature nature of the process offers the potential for use of a wide range of substrates, including selected flexible plastic susbtrates (*e.g.*, polyimides). A wider range of plastic substrates might be employed with a rapid laser-based annealing process,[70] since the semiconducting film on top of the substrate can be selectively and rapidly annealed without substantial heating to the substrate.

An important aspect of this process is that the films are continuous and relatively uniform. A cross-sectional transmission electron microscope (TEM) image (Fig. 13) demonstrates the ultrathin, crystalline nature of a typical $SnS_{1.4(1)}Se_{0.5(1)}$ film spun on thermally oxidized silicon (final anneal/decomposition treatment for this film was at 270 °C for 20 minutes), with average film thickness of ~50 Å – *i.e.*, only 8–10 unit cells thick.[13] Substantial preferred orientation is visible, with the metal chalcogenide layers oriented nominally parallel to the substrate surface (corresponding to the fringes observed in the TEM images). The high degree of solubility, the ability to decompose at relatively low temperature and the small volume of the dissociating hydrazinium species in the current process are all important factors for the formation of high quality,

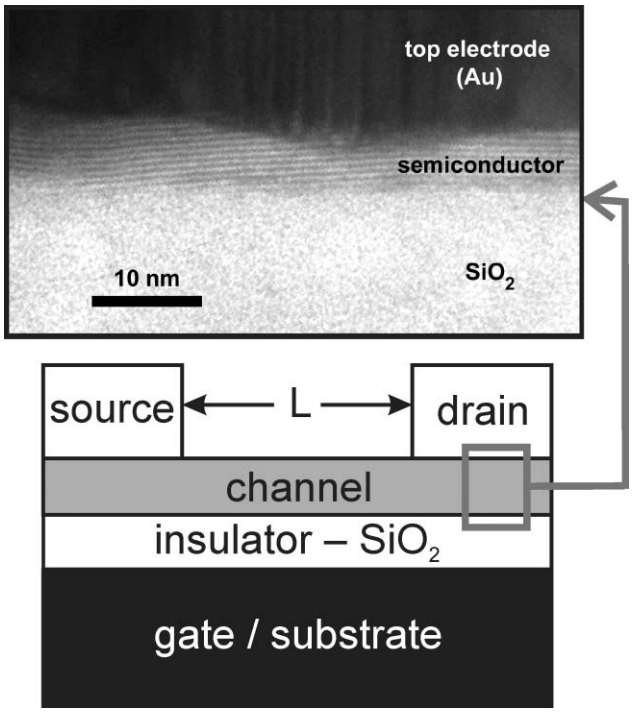


**Fig. 13** The thin-film field-effect transistor (TFT) device (not shown to scale), consists of a heavily *n*-doped silicon wafer as the substrate/gate, a thermally grown $SiO_2$ gate dielectric, the spin-coated chalcogenide channel layer, and patterned Au source and drain electrodes. The magnified region shows a transmission electron microscope (TEM) cross-sectional image of a device based on a spin-coated $SnS_{1.4}Se_{0.5}$ film. Adapted from *Nature*, 2004, **428**, 299 (ref. 13). Copyright 2004 Macmillan Publishers Ltd.

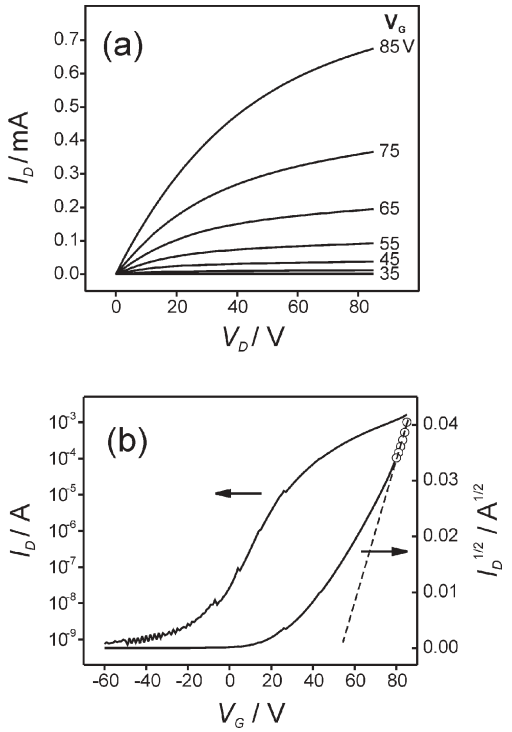


**Fig. 14** Device characteristics for a spin-coated $SnS_{1.4}Se_{0.5}$ chalcogenide channel layer. The gate dielectric consists of 2100 Å of thermally grown oxide and channel length and width are $L$ = 14 μm and $W$ = 250 μm, respectively. (a) Drain current, $I_D$, *versus* drain voltage, $V_D$, as a function of gate voltage, $V_G$. (b) plots of $I_D$ and $I_D^{1/2}$ *versus* $V_G$ at constant $V_D$ = 85 V, used to calculate current modulation, $I_{on}/I_{off}$, and saturation regime mobility, $\mu_{sat}$, for the same device. Reproduced from *Nature*, 2004, **428**, 299 (ref. 13). Copyright 2004 Macmillan Publishers Ltd.

continuous ultrathin chalcogenide films using the spin-coating process.

TFTs based on the spin-coated chalcogenide films have been fabricated with an architecture similar to those described for the organic–inorganic hybrid devices (Fig. 13). In contrast to the organic–inorganic hybrid semiconductors, however, which require a rigorously inert atmosphere during processing, much of the spin-coated chalcogenide film fabrication is performed in air, with the exception of the final channel film anneal (performed in nitrogen). A representative plot of drain current, $I_D$, *versus* drain voltage, $V_D$, is shown in Fig. 14 as a function of the applied gate voltage, $V_G$, for a TFT with a spin-coated semiconductor channel of approximate composition $SnS_{1.4(1)}Se_{0.5(1)}$.[13] The device operates as an n-channel transistor (in contrast to the tin iodide based hybrid devices, which are p-type). Note that the ultrathin nature of the spin-coated films facilitates the large channel current modulation produced by application of $V_G$, as the carrier density modulation is expected to occur primarily in the first few atomic layers, at the interface between the gate insulator and the chalcogenide semiconductor. The current modulation ($I_{ON}/I_{OFF}$), saturation regime field-effect mobility ($\mu_{sat}$), and linear regime mobility ($\mu_{lin}$) are $I_{ON}/I_{OFF} > 10^6$, $\mu_{sat}$ = 12.0 $cm^2\ V^{-1}\ s^{-1}$ and $\mu_{lin}$ = 2.4 $cm^2\ V^{-1}\ s^{-1}$, respectively, for the device operated to 85 V. These device characteristics are representative and are approximately an order of magnitude higher than previous results for spin-coated films. Devices based on tin(IV) sulfide spin-coated films (no selenium) have also been prepared, with saturation-regime mobilities generally in the range of 0.5–1.1 $cm^2\ V^{-1}\ s^{-1}$.[13] The improved device characteristics for the selenide-containing devices likely arise from both the smaller band gap of $SnSe_2$, as well as from the grain structure and film morphology modifications induced by the sulfur–selenium substitution.

In addition to optimizing the thickness and chemical composition of the film (*e.g.*, changing the S : Se ratio), several other factors proved to be important for achieving the high mobilities reported above. TFT operation is primarily sensitive to the first several atomic layers of the semiconductor above the gate insulator (the region in which charge accumulates during application of a bias to the gate), implying that careful attention must be given to making a clean and delamination-free interface between the two layers. Use of freshly distilled hydrazine substantially improved device performance over devices prepared from as-purchased hydrazine (which generally exhibits a yellow coloration). In addition, surface preparation of the substrate was crucial to yield a clean hydrophilic surface. The substrates described above were cleaned using a soap-soaked cotton swab scrub, followed by successive sonication in ethanol and dichloromethane. The substrates were then treated in a "pirahna" bath (1 : 4 by volume of hydrogen peroxide : sulfuric acid) at 100 °C, followed by a deionized water rinse. Substrates were then immediately spun with the hydrazinium precursor solution. Choice of oxide thickness for the gate insulator also significantly affected device results since, for a given applied gate voltage, a higher concentration of carriers in the channel is induced as the thickness of the gate oxide is reduced.[43]

Given the toxic nature of hydrazine, it is clearly desirable to reduce the amount of hydrazine used in the spinning process. To this end, we have recently demonstrated[71] high quality tin chalcogenide films and devices spun using a mixed water/hydrazine solution. In one experiment, 14 mg $SnS_2$, 8 mg $SnSe_2$, and 8 mg S were dissolved in 0.4 ml hydrazine (by stirring approximately 2 hours under a nitrogen atmosphere). After dissolution, 1.6 ml of water was added and the resulting solution was spun in air (3500 rpm), as for the devices prepared from pure hydrazine (final anneal/decomposition treatment for this film was at 260 °C for 20 minutes).[13] Electrical

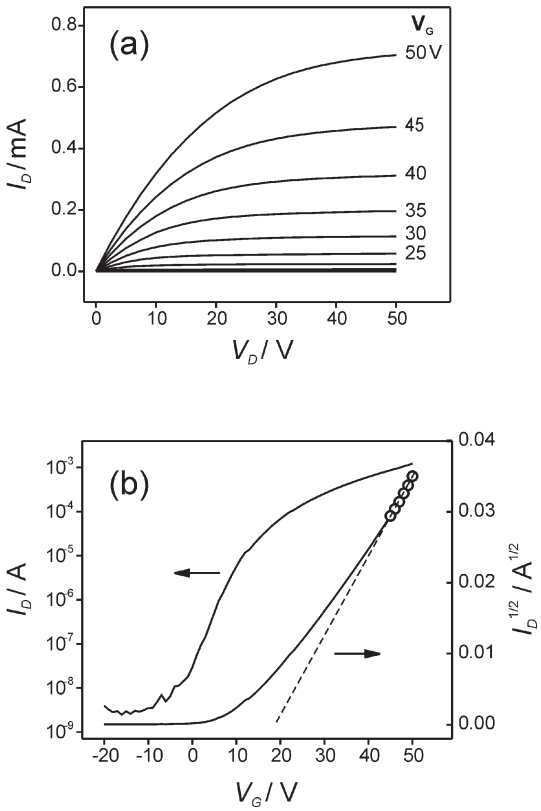


**Fig. 15** Device characteristics for a tin chalcogenide film spun from a mixed water/hydrazine solution (as described in the text).[71] The source/drain contacts are tin, rather than gold. The gate dielectric consists of 1000 Å of thermally grown oxide and channel length and width are $L$ = 95 μm and $W$ = 1000 μm, respectively. (a) Drain current, $I_D$, *versus* drain voltage, $V_D$, as a function of gate voltage, $V_G$. (b) Plots of $I_D$ and $I_D^{1/2}$ *versus* $V_G$ at constant $V_D$ = 50 V.

characteristics for a device prepared from the mixed hydrazine/water spinning solution (Fig. 15) yielded similar results to those achieved from a pure hydrazine solution: $\mu_{sat} = 7.0\,cm^2\,V^{-1}\,s^{-1}$, $\mu_{lin} = 4.3\,cm^2\,V^{-1}\,s^{-1}$ and $I_{ON}/I_{OFF} > 10^5$. In this experiment, lower work function tin source and drain contacts were used rather than gold, leading to better current injection into the devices and higher linear-regime mobilities (although the devices were more difficult to shut off). In addition, a thinner oxide gate insulator was used (1000 Å *versus* 2100 Å) which, along with the lower work function tin contacts, yielded a smaller threshold voltage, $V_T \approx 20$ V (relative to $V_T \approx 55$ V for the device in Fig. 14). While no long-term device stability studies have yet been performed, several devices subjected to 500 gate-sweep cycles ($V_G$ cycled from 50 V to −20V) yielded little or no degradation in either the mobility or current on/off ratio.

The hydrazinium precursor approach described above represents an interesting starting point to address the issue of fabricating high mobility, continuous, ultrathin, metal chalcogenide films using spin-coating (as well as related solution processing techniques). Further issues that need to be addressed, besides trying to attain even higher mobility (as might be expected given the data in Table 1), include trying to identify analogous examples of high mobility p-type chalcogenide films deposited by spin-coating, developing less toxic solvent mixtures to take the place of hydrazine during the spin-coating process, and searching for techniques to further reduce the final anneal temperature required to convert the precursor into the targeted metal chalcogenide semiconductor. All of these issues need to be addressed while maintaining control over film thickness to very thin dimensions and not compromising other semiconducting characteristics.

## Conclusion

Ultimately, any technology developed to solution deposit thin films with mobility in excess of 10 $cm^2\,V^{-1}\,s^{-1}$ should satisfy several criteria to be of practical importance for microelectronic applications. First, the technique must yield uniform and continuous films with ability to control film thickness. Second, the processing should be cheaper than polycrystalline silicon technology (the entrenched technology) for comparable mobility. The technology should also enable new niche technologies for pervasive computing, not readily achievable with traditional poly- or single-crystal silicon technology (*e.g.*, low-cost solution-based deposition on cheap, flexible plastic substrates). Finally, improvement in mobility should not come at the expense of other important device parameters (*e.g.*, on-off ratio, threshold voltage, subthreshold swing).

With the above criteria in mind, the goal of developing solution-processed semiconductors, with mobilities in the range above those currently achievable with organic semiconductors, represents a key challenge for contemporary materials chemistry. In this review, two approaches have been highlighted to address solubility and film formation of inorganic semiconductors, which offer the possibility for higher mobility relative to the organic systems. The first involves layered organic–inorganic hybrids, which combine desirable properties from both components of the structure: The organic component facilitates the self-assembly of the inorganic structure on a substrate (from solution), while the inorganic component offers the opportunity for higher mobility. The initial tin(II) iodide based devices have mobilities of order ~1 $cm^2\,V^{-1}\,s^{-1}$ (similar to the best organic semiconductors deposited by vacuum deposition). Higher mobilities can presumably be envisioned as alternative inorganic frameworks are explored and new semiconducting hybrids are discovered. An alternative approach, based on the decomposition of soluble precursors, enables the deposition of semiconducting metal chalcogenides, a class of materials with large (and in some cases demonstrated) potential for use in electronic devices such as TFTs, solar cells, thermoelectric and memory devices. Despite the early stage of development of these systems, spin-coated chalcogenide films have already yielded mobilities greater than 10 $cm^2\,V^{-1}\,s^{-1}$, clearly demonstrating the feasibility of accessing the higher mobility regime using a low-cost, high throughput process. As for the organic semiconductors, which have undergone tremendous progress over the last 15 years, it is expected that the relatively young and highly promising field of solution-processed inorganic semiconductors will likewise yield many further exciting developments in the years to come, enabling the solution deposition of films and device structures with characteristics that were previously not possible.

## References

1 H. E. A. Huitema, G. H. Gelinck, J. B. P. H. van der Putten, K. E. Kuijk, K. M. Hart, E. Cantatore and D. M. de Leeuw, *Adv. Mater.*, 2002, **14**, 1201.
2 Z. Bao, J. A. Rogers and H. E. Katz, *J. Mater. Chem.*, 1999, **9**, 1895.
3 A. Afzali, C. D. Dimitrakopoulos and T. L. Breen, *J. Amer. Chem. Soc.*, 2002, **124**, 8812.
4 H. Sirringhaus, T. Kawase, R. H. Friend, T. Shimoda, M. Inbasekaran, W. Wu and E. P. Woo, *Science*, 2000, **290**, 2123.
5 H. E. Katz, A. J. Lovinger, J. Johnson, C. Kloc, T. Siegrist, W. Li, Y.-Y. Lin and A. Dodabalapur, *Nature*, 2000, **404**, 478.
6 C. D. Dimitrakopoulos and P. R. L. Malenfant, *Adv. Mater.*, 2002, **14**, 99.
7 X. Duan, C. Niu, V. Sahi, J. Chen, J. W. Parce, S. Empedocles and J. L. Goldman, *Nature*, 2003, **425**, 274.
8 F. Y. Gan and I. Shih, *IEEE Trans. Electron Devices*, 2002, **49**, 15.
9 J. S. Meth, S. G. Zane, K. G. Sharp and S. Agrawal, *Thin Solid Films*, 2003, **444**, 227.

10 B. E. McCandless, A. Mondal and R. W. Birkmire, *Sol. Energy Mater. Sol. Cells*, 1995, **36**, 369.
11 B. R. Sankapal, R. S. Mane and C. D. Lokhande, *Mater. Res. Bull.*, 2000, **35**, 2027.
12 C. R. Kagan, D. B. Mitzi and C. D. Dimitrakopoulos, *Science*, 1999, **286**, 945.
13 D. B. Mitzi, L. L. Kosbar, C. E. Murray, M. Copel and A. Afzali, *Nature*, 2004, **428**, 299.
14 B. A. Ridley, B. Nivi and J. M. Jacobson, *Science*, 1999, **286**, 746.
15 W. E. Howard, *J. Soc. Inf. Disp.*, 1995, **3**, 127.
16 W. G. Hawkins, *IEEE Trans. Electron Devices*, 1986, **33**, 477.
17 For a recent review, see: D. B. Mitzi, *Prog. Inorg. Chem.*, 1999, **48**, 1.
18 D. B. Mitzi, K. Chondroudis and C. R. Kagan, *IBM J. Res. Dev.*, 2001, **45**, 29.
19 D. B. Mitzi and C. R. Kagan, in *Thin-Film Transistors*, ed. C. R. Kagan and P. Andry, Marcel Dekker, New York and Basel, 2003, pp. 475–513.
20 D. B. Mitzi, S. Wang, C. A. Feild, C. A. Chess and A. M. Guloy, *Science*, 1995, **267**, 1473.
21 D. B. Mitzi, *J. Chem. Soc., Dalton Trans.*, 2001, 1.
22 D. B. Mitzi, *Inorg. Chem.*, 2000, **39**, 6107.
23 D. B. Mitzi, C. A. Feild, W. T. A. Harrison and A. M. Guloy, *Nature*, 1994, **369**, 467.
24 K. Yamada, T. Matsui, T. Tsuritani, T. Okuda and S. Ichiba, *Z. Naturforsch.*, 1990, **45a**, 307.
25 S. J. Clark, C. D. Flint and J. D. Donaldson, *J. Phys. Chem. Solids*, 1981, **42**, 133.
26 D. Weber, *Z. Naturforsch.*, 1978, **33b**, 862.
27 (*a*) D. B. Mitzi, C. A. Feild, Z. Schlesinger and R. B. Laibowitz, *J. Solid State Chem.*, 1995, **114**, 159; (*b*) D. B. Mitzi and K. Liang, *J. Solid State Chem.*, 1997, **134**, 376.
28 G. C. Papavassiliou, I. B. Koutselas, A. Terzis and M.-H. Whangbo, *Solid State Commun.*, 1994, **91**, 695.
29 C. Lode and H. Krautscheid, *Z. Anorg. Allg. Chem.*, 2001, **627**, 1454.
30 Z. Xu and D. B. Mitzi, *Inorg. Chem.*, 2003, **42**, 6589.
31 D. B. Mitzi, D. R. Medeiros and P. R. L. Malenfant, *Inorg. Chem.*, 2002, **41**, 2134.
32 D. B. Mitzi, K. Chondroudis and C. R. Kagan, *Inorg. Chem.*, 1999, **38**, 6246.
33 X.-H. Zhu, N. Mercier, P. Frère, P. Blanchard, J. Roncali, M. Allain, C. Pasquier and A. Riou, *Inorg. Chem.*, 2003, **42**, 5330.
34 M. Braun, W. Tuffentsammer, H. Wachtel and H. C. Wolf, *Chem. Phys. Lett.*, 1999, **307**, 373.
35 Z. Xu and D. B. Mitzi, *Chem. Mater.*, 2003, **15**, 3632.
36 D. B. Mitzi, C. D. Dimitrakopoulos and L. L. Kosbar, *Chem. Mater.*, 2001, **13**, 3728.
37 Z. Tang, J. Guan and A. M. Guloy, *J. Mater. Chem.*, 2001, **11**, 479.
38 Z. Xu, D. B. Mitzi and D. R. Medeiros, *Inorg. Chem.*, 2003, **42**, 1400.
39 Z. Xu, D. B. Mitzi, C. D. Dimitrakopoulos and K. R. Maxcy, *Inorg. Chem.*, 2003, **42**, 2031.
40 See, for example: *Physics and Applications of Quantum Wells and Superlattices*, ed. E. E. Mendez and K. von Klitzing, NATO ASI Series B: Physics, Vol. **170**, Plenum Press, New York, 1987.
41 M. Era and S. Oka, *Thin Solid Films*, 2000, **376**, 232.
42 C. R. Kagan, T. L. Breen and L. L. Kosbar, *Appl. Phys. Lett.*, 2001, **79**, 3536.
43 C. D. Dimitrakopoulos, S. Purushothaman, J. Kymissis, A. Callegari and J. M. Shaw, *Science*, 1999, **283**, 822.
44 D. B. Mitzi, C. D. Dimitrakopoulos, J. Rosner, D. R. Medeiros, Z. Xu and C. Noyan, *Adv. Mater.*, 2002, **14**, 1772.
45 W. R. Caseri, H. D. Chanzy, K. Feldman, M. Fontana, P. Smith, T. A. Tervoort, J. G. P. Goossens, E. W. Meijer, A. P. H. J. Schenning, I. P. Dolbnya, M. G. Debije, M. P. de Haas, J. M. Warman, A. M. van de Craats, R. H. Friend, H. Sirringhaus and N. Stutzmann, *Adv. Mater.*, 2003, **15**, 125.
46 J. Britt and C. Ferekides, *Appl.Phys. Lett.*, 1993, **62**, 2851.
47 M. A. Contreras, B. Egaas, K. Ramanathan, J. Hiltner, A. Swartzlander, F. Hasoon and R. Noufi, *Prog. Photovolt. Res. Appl.*, 1999, **7**, 311.
48 Y. Kim, A. DiVenere, G. K. L. Wong, J. B. Ketterson, S. Cho and J. R. Meyer, *J. Appl. Phys.*, 2002, **91**, 715.
49 Ye. P. Sabo, *J. Thermoelectr.*, 2001, **4**, 58.
50 T. Kyratsi, K. Chrissafis, J. Wachter, K. M. Paraskevopoulos and M. G. Kanatzidis, *Adv. Mater.*, 2003, **15**, 1428.
51 I. Friedrich, V. Weidenhof, W. Njoroge, P. Franz and M. Wuttig, *J. Appl. Phys.*, 2000, **87**, 4130.
52 A. P. J. M. Jongenelis, J. H. Coombs, W. van Es-Spiekman and B. A. J. Jacobs, *J. Appl. Phys.*, 1996, **79**, 8349.
53 (*a*) T. Ohta, K. Nishiuchi, K. Narumi, Y. Kitaoka, H. Ishibashi, N. Yamada and T. Kozaki, *Jpn. J. Appl. Phys.*, 2000, **39**(Pt.1), 771; (*b*) T. Ohta, K. Yoshioka, H. Isomura, T. Akiyama and R. Imanaka, *Proc. SPIE Int. Soc. Opt. Eng.*, 1995, **2514**, 302.
54 G. Domingo, R. S. Itoga and C. R. Kannewurf, *Phys. Rev.*, 1966, **143**, 536.
55 T. Shibata, Y. Muranushi, T. Miura and T. Kishi, *J. Phys. Chem. Solids*, 1991, **52**, 551.
56 B. G. Streetman, *Solid State Electronic Devices*, Prentice-Hall, New Jersey, 1980, p. 443.
57 J. A. Beun, R. Nitsche and M. Lichtensteiger, *Physica*, 1961, **27**, 448.
58 B. Tell, J. L. Shay and H. M. Kasper, *J. Appl. Phys.*, 1972, **43**, 2469.
59 T. Nishino and Y. Hamakawa, *Jpn. J. Appl. Phys.*, 1977, **16**, 1291.
60 M. Krunks, O. Kijatkina, H. Rebane, I. Oja, V. Mikli and A. Mere, *Thin Solid Films*, 2002, **403–404**, 71.
61 K. T. Ramakrishna Reddy, Y. V. Subbaiah, T. B. S. Reddy, D. Johnston, I. Forbes and R. W. Miles, *Thin Solid Films*, 2003, **431–432**, 340.
62 K. Y. Rajpure and C. H. Bhosale, *Mater. Chem. Phys.*, 2002, **73**, 6.
63 W. M. R. Divigalpitiya, R. F. Frindt and S. R. Morrison, *Science*, 1989, **246**, 369.
64 G. L. Frey, K. J. Reynolds and R. H. Friend, *Adv. Mater.*, 2002, **14**, 265.
65 S. Dhingra and M. G. Kanatzidis, *Mat. Res. Soc. Symp. Proc.*, 1990, **180**, 825.
66 J. Pütz and M. A. Aegerter, *Thin Solid Films*, 1999, **351**, 119.
67 C. G. Bonnaterre and G. Cauquis, *J. Chem. Soc., Chem. Commun.*, 1972, 293.
68 D. B. Mitzi, manuscript in preparation.
69 B. Eisenmann and J. Hansa, *Z. Kristallogr.*, 1993, **203**, 299.
70 P. G. Carey, P. M. Smith, S. D. Theiss and P. Wickboldt, *J. Vac. Sci. Technol. A*, 1999, **17**, 1946.
71 D. B. Mitzi, unpublished results.